OPTIMIZING SPEED-TO-FLY FOR ENHANCED RANGE OF BATTERY-POWERED AIRCRAFT

H. Spark*, F. J. Silvestre*

* Technische Universität Berlin (TUB), Department of Flight Mechanics, Flight Control and Aeroelasticity, Marchstrasse 12, 10587 Berlin, Germany.

Abstract

We are witnessing increasing pace of commercial developments towards electric propulsion for smaller types of aircraft. At the same time, similarly to electric cars, available range is more limited as with fuel powered vehicles. Different from cars, aircraft design cannot compensate by simply increasing battery size and weight. In this context, flight range optimization becomes crucial, and significant gains can be achieved by optimizing the speed. Existing methods for optimal travel speed that consider the impact of a battery characteristics as Peukert effect and voltage changes on the performance have not investigated varying wind conditions and varying-wind range optimization does not include yet battery effects. As current developments in sustainable, electric aviation focus on smaller and slower aircraft types, wind has a relatively larger impact on the speed-to-fly as compared to twin-jets employed by airline operators. Wind-optimal flight has been viewed as a thrust optimization problem, similar to drag optimization in soaring flight, and has also been investigated with numerical methods that require on-ground evaluation. A more generic approach on speed-to-fly is described in this work by integrating aircraft-dependent aerodynamic and electric propulsion properties in an online evaluation method that makes use of 3D wind information. As motorised glider aircraft with their low power requirement are primary candidates for electric flight, the method is applied on a model of an electric glider. Different degrees of freedom are explored, namely the flight path angle, the throttle and airspeed. The method is based on data that manufacturers could supply or already do supply, making it generally applicable and the effect of considering the dynamic of the battery system is investigated. For the aircraft under investigation, results show that the optimal strategy in zero wind consists of changing between climbing and gliding flight and inclusion of the battery in the evaluation shifts the optimal zero-wind flight condition towards both lower throttle setting and lower climb angle. By including wind-optimal flight and battery effects in an online-method that can be readily evaluated for different types of aircraft, this work contributes to the development of a general method for extending range and enhancing the overall mission capabilities of electric aircraft.

Keywords

Electric Flight, trajectory optimization, guidance

1. INTRODUCTION

Integration of electric propulsion systems is a pivotal advancement towards sustainability and efficiency as the overall propulsion efficiency of electric powered aircraft is much higher than for comparable fuel-powered aircraft. The non-profit organisation ICCT (International Council on Clean Transportation) estimates the efficiency of electric propulsion systems as high as 90 percent (excluding propeller efficiency), and thus to be 2.1 to 3.2 times higher than for fuel-powered aircraft [1]. Research and industry are exploring novel architectures including also hybrid propulsion setups to combine the benefits of electric propulsion efficiency with more dense energy storage. Current projects show that small electric aircraft with less then a dozen seats which are designed for short-haul journeys are at the forefront of electric flight with large full-electric aircraft designs being the exception [2–4]. Several challenges persist in the adaption of batteryelectric aircraft, chief among them being range limitations that directly impact the feasibility and practicality of even short-haul electric flight: The current range limitation is investigated by the ICCT [1] and 9 passenger aircraft is expected to fly $140~\rm km$ missions with the batteries having a specific energy of $250~\rm Wh/kg$.

Besides the limited energy density dictating flight range, electric aircraft are also limited by the power density of batteries [2]. High power battery applications demonstrated in automobiles and model aircraft are often only designed for short power boosts and not for continuous power output [5]. To make matters worse, high power and high energy demands contradict, as shown in Ragone diagrams where energy density decreases with increasing power level [6,7]. This leaves the battery selection process to optimize between energy content and maximum power output, and also may have implication on the aircraft operation as higher discharge currents result in less overall energy delivery of the battery [8–11].

The limited range and power output of electric aircraft underscore the need for specific solutions. One solution is

to favor low flight speeds and high-span wing designs as shown by the list of already flyable, manned electric aircraft in Ref. [4], where the electric aircraft can operate at both low power and close to the slow flight speed at the aerodynamic optimum dictated by the high span. With slow airspeed, the fraction of wind speed in the ground speed and the importance of wind in flight guidance solutions for range-optimal flight increases.

Today, both wind forecasts, e.g. mobile applications for pilots, as well as onboard wind estimation are readily available.

Wind forecast can be used for flight planning. The A-Star algorithm has been used as initial flight path optimization in the TOMATO framework used by Lindner et al. [12] and the capability for cyclic weather udates and re-optimization in flight has been shown [13]. The capability to re-plan the routing of aircraft is also shown by Ottershagen et al. [14] using both an A-Star based approach and dynamic programming as optimization algorithms. Both Ottershagen et al. [14] as well as Langelaan et al. [15] used static battery efficiency or static electrical energy conversion efficiencies.

Fuel-optimal airspeed has been analysed graphically by plotting the power required versus the airspeed as shown by Carson [16] and later Rogers [17]. With the assumption that energy consumption is proportional to power required, and simply defining power required as product of drag and velocity, the best range airspeed graphically determined by the tangential on the required power curve as the maximum lift to drag ratio (L/D) speed.

Carson argued that this best range airspeed might be unacceptably slow, and argued for a higher (Carson-) cruise speed with increased consumption and flight time reduction. In analysing published cruise airspeeds of various models below a weight of 8000 lb weight, Carson concluded that operational practice is to fly close to this Carson cruise speed or even faster and that typically cruise settings are close to $75\,\%$ power level.

For fuel-powered (and high-speed) airliners, a more detailed model for fuel-optimal flight analysis can be obtained by defining a thrust-specific fuel consumption as functional of thrust setting and Mach-Number [18]. With available models of specific fuel consumption, the impact of wind on aircraft range was investigated and it was again stated that typical operation is at off-optimal range speed, using faster airspeeds [19].

In the trade-off between travel speed and energy consumption, the restrictions of electric aircraft can arguably tip the scale towards best L/D flight.

Thrust specific fuel consumption methods are not applicable to electric aircraft, which leads to the development of thrust specific (supply) power consumption [20]. Opposed to fuel-optimal flight, battery-optimal flight is dependent on the characteristics of the power source as well. However, the influence is under debate, with some authors highlighting the effect of the battery on the optimal trajectory and airspeed [9, 10, 21, 22] and others neglecting it, arguing voltage changes and internal resistance are small [11]. Primarily, the effect of capacity reduction at high discharge rates is discussed, with the literature pointing out that this is only modelled correctly

with the Peukert effect if discharge is constant [8, 9]. Secondarily, the effect of voltage drop under load in the battery model is discussed, with lower voltages in flight reducing the best range speed [10,11] as was the effect of the battery internal resistance that improves simulation results but did not allow analytic solution for best range speed [23]. A visual representation of the battery effect on speed to fly is given by Avanzini and Giulietti [22], as they interpret the Peukert effect as moving the best range cruise on the power required curve between the points of minimum power required and minimum drag, latter in case of an ideal battery with Peukert coefficient at unity and being the traditional best range condition for piston propeller aircraft. Settele [24] evaluated the battery effect on the optimal trajectory and also described a criterion of optimality as well as a search grid approach of parameters to arrive at local optima as the best range and to be able to show those optima to the pilot. However, the listed contributions to battery-optimal flight that include battery effects besides static efficiency have not yet considered wind.

With different best-range airspeeds at different wind conditions and no forward-looking, thus not considering future information of the wind profile directly ahead, an approximate optimal strategy is to fly the locally optimal airspeed at each instant of time, thereby connecting all local optima of consumption per range. Langelaan [25] implemented a control law to follow such steady-state local optima. Also, for electric flight Langelaan et al. [15] minimised electric power required per ground speed, developing node to node optimal flight speed and power reference with gradient-descent optimization, then handing the pilots the results. However, effects of the battery were not considered. Flight path reference was generated also, to change altitude and exploit favourable wind conditions. Thus, the optimization included the effect of the flight path angle reference on the optimal airspeed and power per flight plan segment. Those results were updated while the pilot was airborne, but the updates were not generated onboard as direct reaction to measured wind.

Using only airspeed optimization, one would lose the effect of flight altitude and position on both the aircraft performance characteristics as well as on the effect of altitude and position on the wind itself.

If aircraft performance and wind conditions are known and dependent on altitude and position, a flight path reference in combination with airspeed optimization should be evaluated. To this end, the Chair of Flight Mechanics, Flight Control, and Aeroelasticity (FMRA) at TU-Berlin has investigated methods of wind-aware trajectory optimization under consideration of battery performance related effects. The method generates waypoint information for battery-powered range-optimal flight, including references for the flight path angle and airspeed. A table lookup for the optimal flight speed depending on the local wind was used, and a tracker commanded the aircraft to follow the airspeed references [26]. A visualisation of a planned trajectory defined by waypoints is shown in Fig. 1.



FIG 1. Trajectory planning results in Bavaria, with planned path shown blue

However, instead of table lookups, online speed-to-fly and power setting adaptions can be generated by extending the graphical approach of Carson with powertrain efficiency models to a) derive thrust specific power consumption necessary for electric aircraft analysis and b) extend the efficiency model with a battery model, changing from power required optimization to minimising state of charge per ground distance.

Thus, the objective of the present work is to establish an optimization method that uses performance data of propeller, motor and battery in the onboard calculation of the optimal speed to fly and throttle setting. The method is comprehensively described by extension of Carson's graphical approach. It includes the effect of 3D wind on the required energy and on the ground speed. The described solution is able to use flight path reference data to adhere to a planned flight profile, making it applicable for varying flight path angles including horizontal flight. As modular representations of propeller, motor and battery are used which are based on measurement and/or manufacturer data, the method is generally applicable for differing aircraft types.

2. METHOD DESCRIPTION

The method relies on quasi-steady aircraft performance evaluations with both airspeed V and flight path angle γ at equilibrium:

(1)
$$\dot{V} = \frac{1}{m} (T \cos \alpha - D - mg \sin(\gamma + \alpha_w)) = 0$$

- $(2) \qquad \dot{\gamma} = 0$
- $(3) \qquad \dot{\psi} = 0$

Wherein m is the aircraft mass, g the gravitational acceleration, ψ the heading angle and α_w the vertical angle from flight path (x-) axis to aerodynamic (x-) axis [27]. To find steady-state optima online, the consumption model uses a thrust computation that accounts for wind effects and varying flight path angles γ as well as changing air densities $\rho.$ The model uses the common definitions of lift and a quadratic drag polar. The effect of thrust on the aerodynamic z-axis is neglected as in

Ref. [27]:

(4)
$$L = mg\cos(\gamma + \alpha_w) = \frac{1}{2}\rho V^2 SC_L$$

$$D = \frac{1}{2}\rho V^2 S C_D$$

(6)
$$C_D = C_{D_0} + kC_L^2$$

 C_L being the lift and C_D drag coefficients, respectively. Aircraft parameters used for inital method evaluation are given in Tab. 1.

To include the effect of wind on the thrust required at constant airspeed as expressed by Eq. 1, first body components are derived by rotating lift and drag with angle of attack α . With the pitch angle θ defined as

(7)
$$\theta = \gamma + \alpha_w + \alpha$$

The wind effect on pitch is included by the wind-induced angle of attack α_w

(8)
$$\alpha_w = \frac{1}{V} \left(\sin \gamma \cos \chi u_W + \sin \gamma \sin \chi v_W + \cos \gamma w_W \right)$$

with χ being the course and u_W , v_W , w_W the north, east and downward wind components [27]. With defining the wind direction χ_W as the direction the wind of horizontal velocity magnitude V_W is flowing towards, α_w can be expressed as

(9)
$$\alpha_w = \frac{1}{V} \left(\cos(\chi_W - \chi) V_W \sin \gamma + w_W \cos \gamma \right)$$

Lastly, the pitch effect on thrust required to satisfy the equilibrium of Eq. 1 is given by

(10)
$$T = F_{xb,aero} + mg\sin\theta$$

with the index b indicating body coordinates.

2.1. Extended Three-Degree-of-Freedom Model

The following description of the consumption model starts on the basis of a known thrust. Propeller and motor efficiency data are oftentimes supplied as charts. The propeller data may consist of propeller efficiency η_{prop} and propeller power coefficient c_P over a range of advance ratios J

$$(11) J = \frac{V}{nd}$$

The advance ratio depends on propeller diameter d, rotational speed n and airspeed V. Thrust coefficients c_T can be defined as:

(12)
$$c_T = \frac{\eta_{prop} c_P}{J}$$

Here, instead of using proprietary propeller and motor data, the propulsion efficiency is calculated based on propeller and motor efficiency parameters given by Langelaan

et al. [15]. With the thrust needed defined as

$$(13) T = c_T \rho n^2 d^4$$

and at a given airspeed V, the set of allowable rotational speeds n is evaluated to give the advance ratio J and to match the thrust condition. This also determines the power coefficient c_P and propeller input power P as well as the efficiency of the propeller by using Eq. 12.

$$(14) P = c_P \rho n^3 d^5$$

With motor efficiency η_m , the electric power need of the propulsion system P_{el} is calculated as

(15)
$$P_{el} = \frac{P}{\eta_m}$$

from which the incremental loss of battery state of charge (SoC) is calculated in the following, based on lithium battery parameters given by Donateo et al. [28] and setting nominal current I_{nom} of $22~\mathrm{A}$.

To calculate the loss of SoC, from the last SoC value the open circuit voltage U_{OC} is determined with battery-technology dependent parameters E_0 , A, B, K as taken from Ref. [28] as:

(16)
$$U_{OC} = E_0 - \frac{100K}{SoC} + Ae^{-BC_{nom}\left(1 - \frac{SoC}{100}\right)}$$

wherein E_0 is a constant voltage, K accounts for polarisation and A and B both account for an exponential zones amplitude and range. To account for internal battery resistance R_{bat} and with the open circuit voltage U_{OC} defined, the current draw I is

(17)
$$I = 1/(2R_{bat})(U_{OC} - \sqrt{(U_{OC}^2 - 4R_{bat}P_{el})})$$

(see also Refs. [29, 30]). From this current I, the effective discharge current I_{eff} is computed with the Peukert effect which is described in Refs. [21, 28, 31, 32]:

(18)
$$I_{eff} = I\left(\frac{I}{I_{nom}}\right)^{n_b - 1}$$

$$S\dot{o}C = -100 \frac{I_{eff}}{C_{nom}}$$

With the factor 100 representing the conversion from unit SoC to percent.

2.2. Extending The Power Required Polar

For propeller driven aircraft, a common advise on speed-to-fly for maximum range is that the drag or drag-to-lift ratio (lift equals weight in cruise) should be minimised [16,22,33]. Energy expenditure dE/dt is assumed proportional to power. Power is also assumed proportional to drag times velocity

(20)
$$\frac{dE}{dt} = P = DV$$

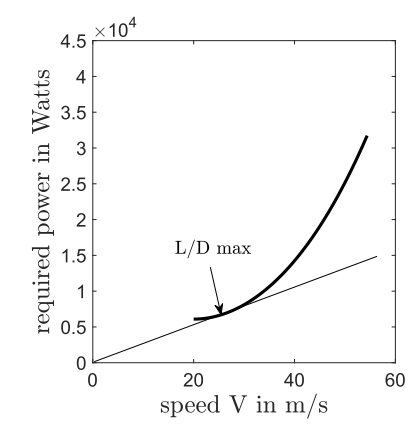


FIG 2. Best L/D in P-V coordinates

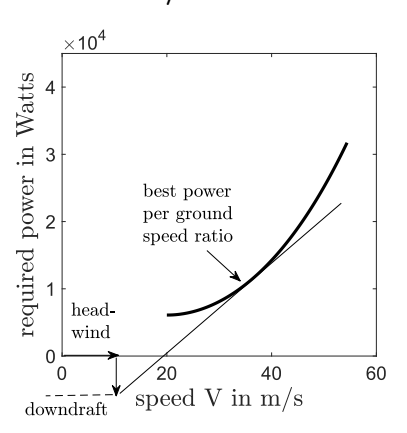


FIG 3. Best range considering wind

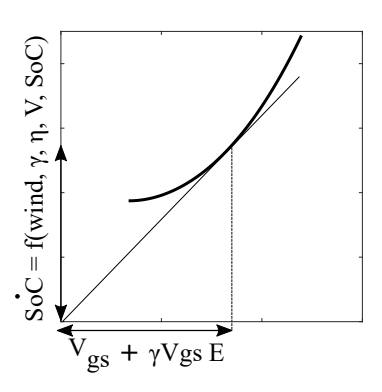


FIG 4. Best range considering consumption models including battery

©2024

4

TAB 1. Example Aircraft Parameters

| Parameter | Value |
|---|------------------|
| Wing area | 15 m^2 |
| Mass | 900 kg |
| Battery capacity | 113.26 Ah |
| Battery (SoC 100%) open circuit voltage | 407.5 V |
| Maximum speed | 70 m/s |
| Zero-lift drag coefficient C_{D0} | 0.01 |
| Zero-lift coefficient C_{L0} | 0.3 |
| Lift slope C_{Llpha} | 6 |
| Lift-dependent drag coefficient k | 0.015 |
| Propeller diameter d | 3 m |
| Max motor power | 70 kW |
| | |

Assuming this, the derivative considering range s is

(21)
$$\frac{dE}{ds} = \frac{dE}{dt}\frac{dt}{ds} = \frac{P}{V} = D = \frac{W}{L/D}$$

which explains that the best range speed is the one that maximises L/D, i.e. minimises drag. Also, Eq. 21 leads to conclude that the best range speed can be found graphically by a tangent in the P-V coordinate system, see Fig. 2. The construction of this tangent is shown by Rogers et al. in [17].

However, horizontal wind changes the ground speed V_{gs} , thus changing the best rate dE/ds. Horizontal wind influence can be graphically constructed with the P-V diagram as shown in Fig. 3. Here, the horizontal placement of the tangent changes to reflect V_{gs} . The ground speed can be calculated using the law of sine in a triangle defined by the angles $A,\ B$ and C as in Ref. [34]:

$$(22) A = |\chi_w - \chi|$$

(23)
$$B = \arcsin(V_W \frac{\sin(A)}{V})$$

$$(24) C = \pi - (A+B)$$

$$(25) V_{gs} = V \frac{\sin(C)}{\sin(A)}$$

Positive vertical wind, defined downwards, increases the required power for the same velocity and flight path angle. To include the effect of vertical wind in the graphical construction of the speed-to-fly, the energy rate induced by the vertical wind can be expressed in un-accelerated level flight, as in Ref. [27]:

(26)
$$\dot{E} = GV\alpha_w = -V(\alpha_w - \gamma_{gl})L$$

with G being gravitational force and γ_{gl} the glide angle. However, calculating the additional power required that is induced by vertical wind directly from speed and α_w , one ignores the changes in propulsion efficiency and any effects on the battery that result from the now changed power required. Here, by rotating the lift, drag and gravitational force into the body coordinates, the effect of the wind angle α_w is incorporated before the thrust is input

TAB 2. Speed-to-fly variations

| Variation | γ | η_t | V |
|-----------|----------|----------|----------|
| Variant A | variable | variable | variable |
| Variant B | fixed | variable | variable |
| Variant C | variable | fixed | variable |

to the consumption model. Thus, the effects of changed power required are combined with the efficiency models to result in the state of charge change per unit ground speed, see Fig. 4. Note, that when taking the propulsion and battery effects into account, the tangent to the best range does generally not need to coincide with the traditional solution of the best range speed for piston aircraft, that is the minimum drag speed [22].

2.3. Considering Climb Rate

Additionally to the above-mentioned consideration of horizontal and vertical wind in the required power analysis for level flight, the change in altitude is also considered in finding the best operation point as positive altitude gain can be converted to range without power input. Therefore the ground-speed axis is extended to include range gain from climb rate. As electric aircraft have comparatively low climb performance as result of the limited power available, the horizontal distance travelled in climb is considerable such that flight condition of best climb rate is not guaranteed to give the best range.

Switching from a graphical view of the problem to discrete implementation, the range gain by increased potential energy is included in a performance evaluation by using the expected glide ratio E_{exp} which is calculated from the aircraft polar and the horizontal wind, assuming it is mostly constant in flight. The best performance is then described by the maximum

(27)
$$\max(\frac{V_{gs} + \gamma V_{gs} E_{exp}}{\dot{SoC} = f(\eta, T(\mathsf{wind}, V, \gamma), SoC)})$$

This performance is evaluated by sweeping sets of flight path angles and airspeeds instead of graphical construction of a tangent as described above. This circumvents issues of data interpolation and filtering in constructing the tangential from differentiating the battery power draw. Note that only the horizontal wind components influence the glide ratio evaluation. This design choice is due to the vertical wind being volatile with long-term mean close to zero whereas the horizontal wind reflects better the mean wind conditions. Equation 27 extends the maximum range criterion with vertical flight segments as described by Settele [24] with a general formulation that includes wind effects on both the required thrust and thus the operation points and associated efficiencies in the propulsion models as well as on the expected glide ratio.

©2024

5

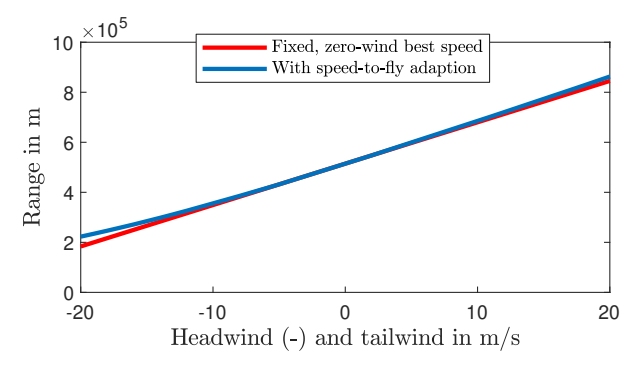


FIG 5. Horizontal wind: Benefit of speed-to-fly

2.4. Selecting Degrees of Freedom in The Optimization

As it was considered sensible to always optimize the airspeed, resulting possible variations to be evaluated prescribe either no value, the flight path angle γ or the throttle setting, see Table 2. Although influencing multiple flight parameter references, the variations are referred to as speed-to-fly variants in the following. With those variants, only fixing the power to an expected climb value (C in Fig. 2) or fixing the flight path angle (B) in the construction of the tangent lead to a (more or less direct) following of the planned flight path angle reference. Note that the thrust setting is applied directly from the optimization response, i.e. no closed-loop flight path control is used. This is necessary for method C and it allows for pitch controlling only airspeed resulting in faster airspeed control while using power in a feed-forward manner.

3. RESULTS

Before the variations are evaluated in detail, the general influence of speed-to-fly adaptions on range is shown for varying horizontal wind in Fig. 5. Head- and tailwind are significantly changing the achievable range. Here, speed-to-fly variant B with zero flight path angle reference $\gamma(B)$ is used. Especially in headwind, not adapting to the speed-to-fly rule equals loss of up to 21.4 percent of range at $20~\rm m/s$ headwind compared to flight with best zero-wind range speed at $31.1~\rm m/s.$ In tailwind, achievable range benefits are minor with around $2.1~\rm percent$ in $20~\rm m/s$ tailwind.

Flight path angle, throttle and airspeed reference in cruise and climb settings for a range of vertical winds are reported as results of the speed-to-fly variations A, B and C. The results are generated at an altitude of 0 m for both cruise and climbing flight. The influence of the battery system on the optimal range airspeed is evaluated. To this end, additional results are presented with battery effects excluded. Exclusion of battery effects is done by using 100 percent SoC to calculate the open circuit voltage, setting unit Peukert coefficient and lastly ignoring battery resistance by using

$$(28) I = \frac{P_{el}}{U_{OC}}$$

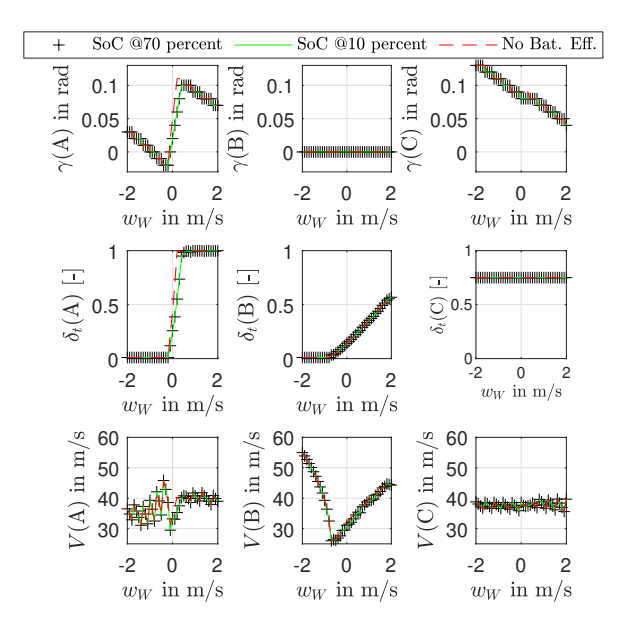


FIG 6. Cruise optimization results, values for different SoC levels are identical

making the consumption \dot{SoC} only dependent on the aerodynamic properties and the motor and propeller.

3.1. Cruise: Level Flight

Flight speed, throttle setting and resultant flight path angles for cruise are shown in Fig. 6 where negative vertical wind velocities w_W indicate updraft.

The results either include the battery parameters as given by Donateo et al. [28] (with Peukert-effect), or exclude battery effect. Only in variant (A) effects of the battery are visible in Fig. 6. In the other cases, results for different SoC values at 70 percent or 10 percent are mostly overlapping with the results excluding the battery, with minor deviations showing higher airspeed in variation B at some evaluation points. In variation A however, the exclusion of battery effect changes the optimal flight condition drastically. When evaluating zero wind, Fig. 6 shows the optimal condition without battery is at a flight path angle of 0.05 rad (2.86 deg) with 43 percent of throttle and resulting in a zero-wind range of 563.91 kmunder the assumption that gained altitude can be used as glide range. This result demonstrates a higher climb angle and and higher throttle setting as optimal with battery effect in the current setup, as well as higher airspeed. With battery effect, variant A is resulting in a zero-wind range of 531.37 km. For variant C, the throttle reference of 75 percent leads to higher airspeeds as with variant A, as the degree of freedom to reduce throttle to near-zero is not given.

Minimum throttle is set at 0.01 to avoid division by zero.

3.2. Climb

6

As the best zero-wind climb angle evaluated with variant A in Fig. 6 is 0.02 rad (1.146 deg), this climb angle is selected as reference for variant B and the corresponding throttle setting of 26 percent is set as reference for

©2024

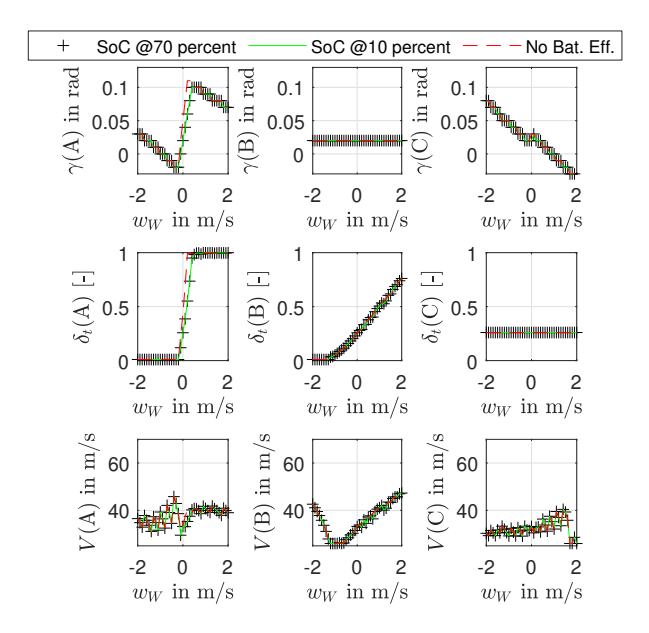


FIG 7. Climb optimization results, values for different SoC levels are identical

variant C. Again, this setting deviates when the battery effect is ignored. Figure 7 shows the results for climbing flight. By comparing to the cruise optima it can be seen that variant B now has a smooth speed-to-fly profile as it evaluates to lower airspeeds in high updraft and speed as well as throttle are continuously increased to compensate negative impact of vertical wind (downdraft). Also, without battery effect in variant B, the best airspeed and throttle setting are slightly higher, starting from downdraft of 0.5 m/s with maximum offset of 3m/s and 5 percent throttle compared to the identical results of the 10 and 70 percent SoC runs. For variant C, the lower power setting determined with variant A results in lower optimum airspeeds that also increase with downdraft. General observations are that variant A has a small transitional area between flying with near-zero SoC consumption in updraft, even at the expense of small altitude losses, whereas variant B enforces the flight path angle in updraft, potentially increasing airspeed in level flight and with variant C mostly the power available is used to maximise the climb angle.

3.3. Statistical Evaluation

For statistical evaluation, the throttle and climb reference of 0.26 and 0.02 rad are again used to initialise variants B and C with the optima of variant A.

For reference, the results without wind are shown in Fig. 8. It can be seen that the performance for both A and C is equal (as C was initialised with the optimum of variant A) and the zero path flight angle prescribed in variant B is sub-optimal, thus switching between climbing and gliding segments of flight is evaluated as more beneficial. Using constant-length segments (1000 m) with constant Gaussian-distributed randomised wind condition per segment, the aforementioned three variants are used to guide a performance model of the aircraft in cruise ($\gamma_{ref}=0$).

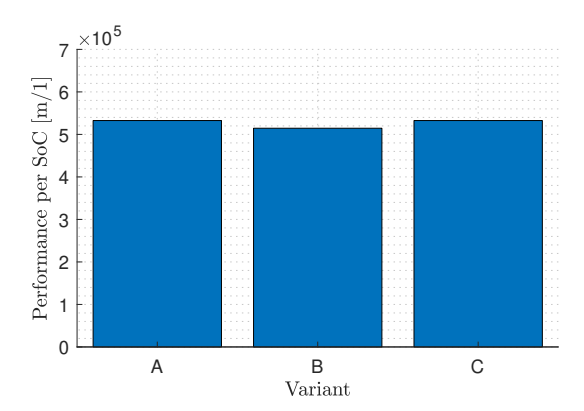


FIG 8. Zero wind evaluation of cruise performance

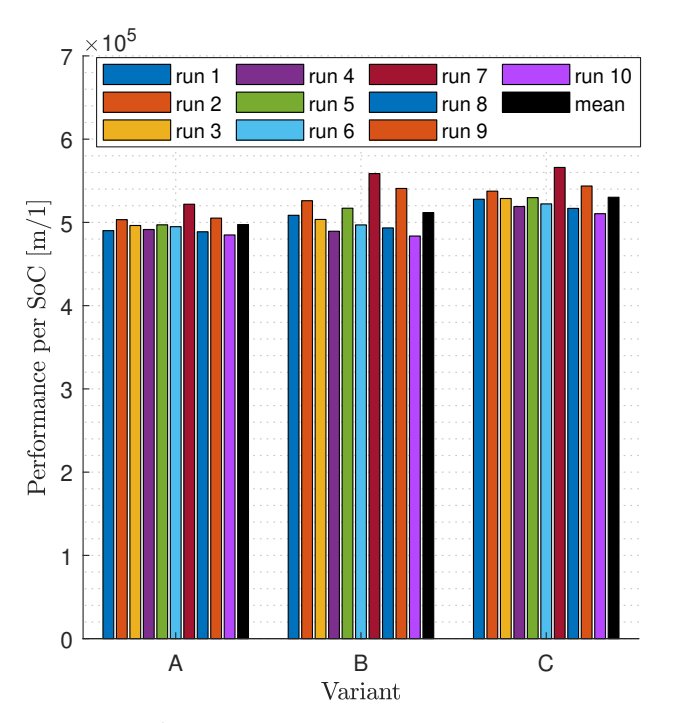


FIG 9. Variation of performance in cruise

The wind is described by

(29)
$$w_W \sim N(\mu, \sigma) : \mu = 0, \sigma = 0.5 \text{ m/s}$$

(30)
$$V_W \sim N(\mu, \sigma) : \mu = 0, \sigma = 4 \text{ m/s}$$

with the standard deviation reflecting that most of the vertical wind magnitude encountered is below the horizontal wind magnitude. The segments are initialized at 70 % SoC.

3.4. Statistical Evaluation of Cruise: Level Flight

Wind-direction as well as flight path are pointing northwards (0 deg). Note that to compare performance of the enforced level flight with variant B, the variants A and C add to the performance the gained altitude times the mean glide ratio considering the horizontal wind representations and based on the aerodynamic properties listed in Tab 1. From the quasi-steady responses in the constantlength segments, the altitude information is also gathered to reward or penalise gain or loss of altitude compared to

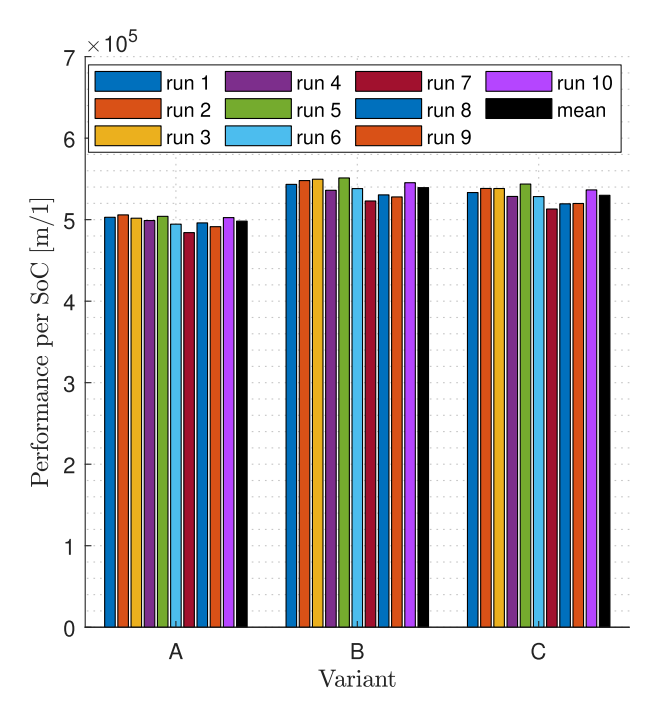


FIG 10. Performance in climb

the reference path by the performance

(31)
$$J = \frac{\sum \Delta s + \sum \Delta h E_{exp}}{\sum \Delta SoC}$$

where s is the constant distance per segment of 1000 m, h is the altitude and unit SoC represents one full battery charge.

The performance thus represents the distances one can fly with a full battery, using the variations A, B ($\gamma = 0$) or C ($\delta_t = 0.26$) in the Gaussian wind distribution. The resultant performance of ten runs of each 200 segments with randomised wind representation are shown in Fig. 9. With random representations of vertical and horizontal wind the results for the free optimization variant A, the fixed-flight-path variant B and the fixed throttle variant C which exhibit nearly the same performance. There is no benefit to variant A, although there was in the static evaluation, see Fig. 8 and all individual segment performances of variant A exceed those of the other methods, showing that the optimum of the average of the ratios is not the global optimum (that is the ratio of the averages). Latter only can be evaluated a posteriori, with knowledge of the wind conditions. Of the range (around 500 km) in these investigations, only about 300 km are usable. That is due to initial SoC consumption for start and climb (over ten percent in case of 1000 m flight altitude) and the requirement to arrive with more then 30 percent SoC to have go-around capacity and to not damage the battery cells by deep discharge in the normal operation.

3.5. Statistical Evaluation of Climbing Flight

As established, climbing flight increases the range performance. Thus, for fair comparison, variant B is initialised with the climb reference 0.02 rad of variant A. Again, throttle for variant C is set to 0.26. The results are shown

TAB 3. Ratios: Variant A

| | run 1 | run 2 | run 3 | \sum |
|---------------------------------|--------|--------|-------|----------|
| Δ h [m] | 60 | 20 | -20 | 60 |
| Δ s [m] | 1000 | 1000 | 1000 | 3000 |
| Δ SoC [-] | 0.7290 | 0.3414 | 0 | 1.07039 |
| $R \; [\mathrm{m}/\mathrm{1}]$ | 452225 | 543367 | inf | inf |
| $RA \; [\mathrm{m}/\mathrm{1}]$ | | | | 502584.1 |

TAB 4. Ratios: Variant B

| | run 1 | run 2 | run 3 | Σ |
|------------------|--------|--------|--------|-----------|
| Δ h [m] | 0 | 0 | 0 | 0 |
| Δ s [m] | 1000 | 1000 | 1000 | 3000 |
| Δ SoC [-] | 0.2554 | 0.1932 | 0.1224 | 0.5709 |
| $R \; [m/1]$ | 391585 | 517575 | 817289 | 1726448.7 |
| RA [m/1] | | | | 525451.9 |

in Fig. 10. Again, the performances are close. However, the local optima in variant A do not lead to the optimal solution when evaluating the 2000 flight segments with the Gaussian wind distribution.

From the results one can conclude that following all local minimal without restrictions - as in variation A - does not lead to the best range overall. Variant A optimizes the average of the ratios by maximising each ratio R

(32)
$$R = \frac{1000 \text{ m} + \Delta hE}{\Delta SoC}$$

whereas the statistical performance is evaluated for 200 segments as the ratio of the averages RA

(33)
$$RA = \frac{\sum_{i=1}^{200} (1000 \text{ m} + \Delta h_i E)}{\sum_{i=1}^{200} \Delta SoC_i}$$

The sum of the ratios R and the RA are generally not the same.

As can be seen from comparing Table 3 and 4, individual ratios R mark variant A as best. But, when evaluating the RA, variant B is better. The mean glide ratio E_{exp} in the three wind instances was 39.66.

3.6. Speed-to-fly in Gust Reaction

A planning program for optimal flight paths and airspeeds has only information of the predicted wind, it cannot include local phenomena as vertical gust from thermals (only large impact area phenomena as orographic lift at mountain slopes can be accessed by the wind prediction data). Also, the planner cannot compensate for locally differing horizontal wind strengths, i.e. non-precise forecasts.

Here, as local effect a gust (downdraft) with one-minuscosine transitions is shown. As in the previous the speedto-fly results indicated similar performances between the three variants, variant B is chosen for implementation in a nonlinear simulation due to its ability to hold a

©2024

8

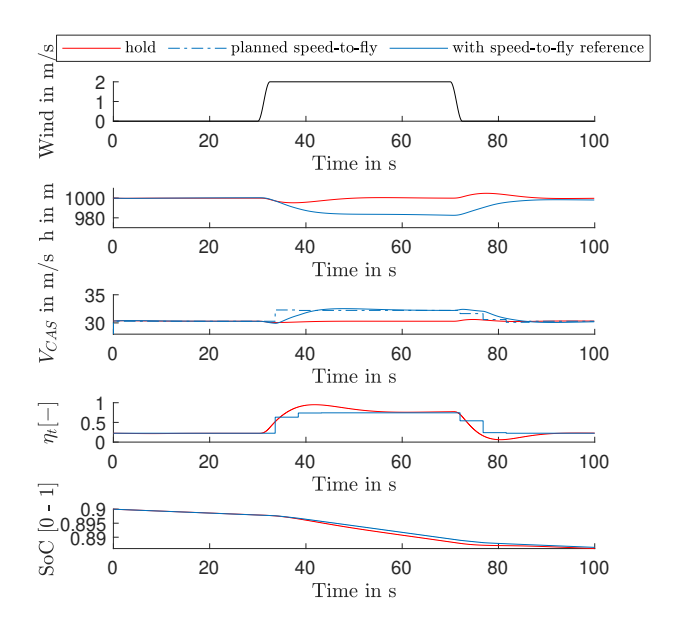


FIG 11. Speed-to-fly in gust

planned flight path angle in varying wind conditions and its smooth speed-to-fly results that show increasing air-speeds with increasing downdraft. Using a different, proprietary dataset for the aircraft performance, the resultant optimal speeds differ from the results previously shown

Fig. 11 shows the vertical wind strength, altitude, the reference of optimal speed as well as actual speed. The aircraft is controlled by a total energy control system (TECS, part of the system described in [35]) with a speed control time constant of 6.67 s. Both the aircraft reaction with the controller in airspeed and altitude hold (indicated red) as well as the reaction of the wind-optimal control (blue) are shown. The gust input starts at 30 s. Initially both controllers start at the same airspeed, the best range airspeed at zero wind for this aircraft. It can be seen from the altitude response that the holdcontroller stabilises the aircraft to the hold-values in a matter of few seconds. This is achieved by throttle input. The wind-optimal control initially loses altitude in downdraft, and only regains altitude as the gust input steps back to zero. Distinct steps in the throttle response of the wind-optimal control are visible - it stabilises at a similar throttle setting as the hold-controller, with a residue altitude offset of 1.35 m to the reference altitude at end of simulation. Both control approaches use nearly the same amount of battery energy, expressed as SoC. However, due to increased airspeed the wind-optimal control covers more distance, namely $3.263~\mathrm{km}$ compared to 3.178km with the hold-controller.

3.7. Flight Mission

The coupling between planned altitude profiles and the speed-to-fly optimization is further investigated. A mission planner [26] generates a reference flight path from the centre of Berlin to Schwerin (EDOP - Parchim) that is coupled to speed-to-fly variant B. Variant B determines

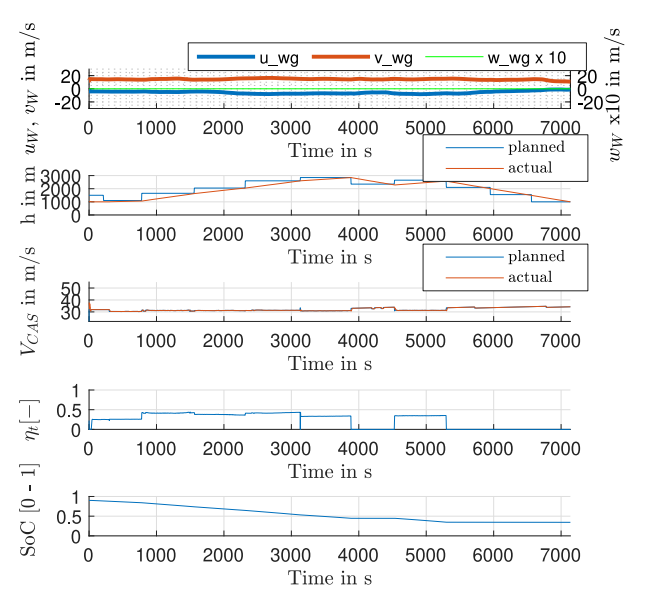


FIG 12. Berlin - Schwerin without turbulence

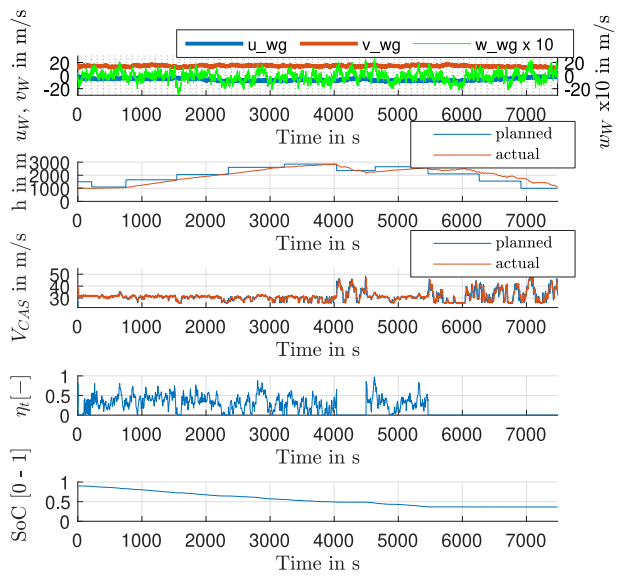


FIG 13. Berlin - Schwerin with (+) turbulence

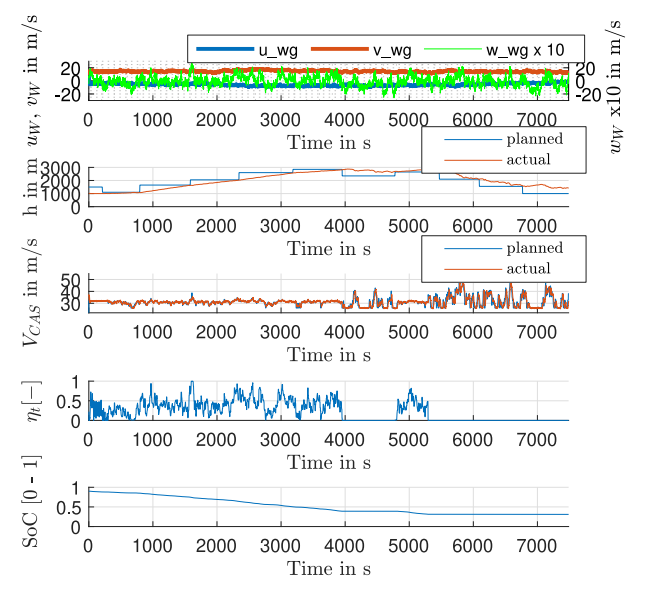


FIG 14. Berlin - Schwerin with (-) turbulence

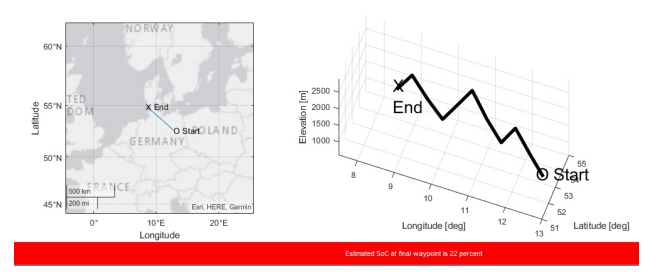


FIG 15. Planner Results: Berlin (Bienenfarm) - Sylt

airspeed and throttle for the flight mission. Position- and altitude-dependent wind is loaded from forecast data. In Fig. 12 simulation data with position-dependent wind is shown. The wind contributes to headwind mainly. The altitude closely follows the planned profile which is characterised by changing between climbing and gliding segments of flight (sawtooth profile). Only few changes in airspeed are applied, mainly in the transitions from climb to glide. Throttle is used in a quasi-static manner as the wind is mainly constant. To evaluate the influence of additional turbulence to the speed-to-fly optimization, a position-dependent (Dryden) turbulence profile is added. To diminish mean positive or negative vertical wind influence on performance, the profile is applied with negated direction also. Figure 13 shows the results for the nonnegated (+) profile. Turbulence has influence on the vertical wind mainly, only minor changes to the horizontal wind are visible. The altitude profile shows temporary level or positive flight paths in glide segments where throttle is zero. Airspeed commands by the speed-to-fly variant B and reactions of the aircraft change rapidly, with higher variance in the glide segments. The flight ends above the planned altitude. Figure 14 shows the results for the negated (-) profile. The flight ends at even higher altitude. When comparing throttle results from the speed-to-fly variant B, the throttle reacts opposed to the (+) turbulence, visible at 1000 s and 5000 s for example. Both simulated flights show the ability of speed-to-fly variant B to closely follow the planned altitudes.

Opposed to the headwind-simulation starting from Berlin to Schwerin which is around 150 km, the capability of electric flight is shown in tailwind condition with wind from the east at 10~m/s and flight from north of Berlin (EDOI - airfield Bienenfarm) to Sylt (EDXW). The planner can be used to evaluate the feasibility of such flights. Here, the calculated SoC at Sylt at 1000~m altitude is 22~percent, with the flight profile showing again the sawtooth-type, periodic switch between climbing and gliding flight. The decision if the final SoC is enough is then for the pilot to evaluate - otherwise the flight can be postponed if even more tailwind is predicted.

4. DISCUSSION

This section evaluates the speed-to-fly generation as well as the coupling to flight path data from flight plans as well as the behaviour in turbulence.

TAB 5. Flights from Berlin to Schwerin

| Field | Result |
|------------------------------|-----------|
| SoC Turb off | 0.344 [-] |
| final altitude Turb off | 1001.7 m |
| SoC Turb on $(+)$ | 0.364 [-] |
| final altitude Turb on $(+)$ | 1105.6 m |
| SoC Turb on (-) | 0.310 [-] |
| final altitude Turb on (-) | 1404.4 m |
| mean SoC Turb $(+/-)$ | 0.337 [-] |
| mean Altitude $(+/-)$ | 1255 m |

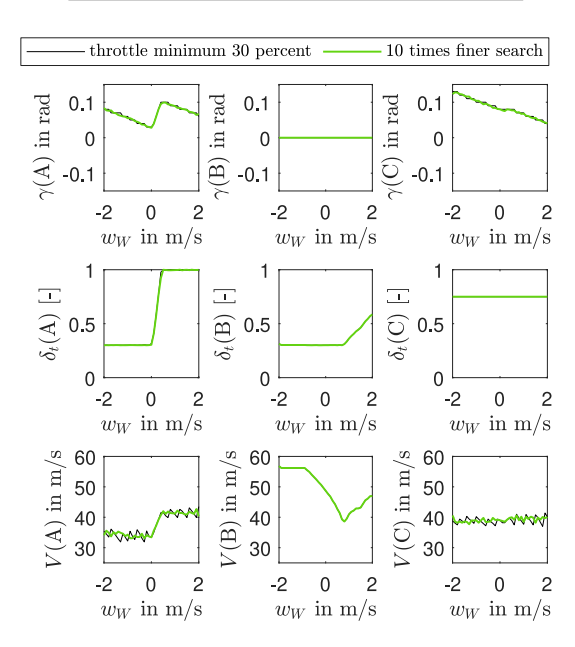


FIG 16. Effect of parameter variation

4.1. Discussion of Discretisation Parameters

The speed-to-fly settings calculated with variant A have shown a degree of ripple, visibile in Figs. 6 and 7. Firstly, this can be attributed to the method optimizing for zerothrottle conditions in updraft as most ripple is visible in the range of zero throttle. When setting minimum throttle to 30 percent, that ripple is reduced, shown in Fig. 16. Also, with minumum of 30 percent throttle, variant B shows even higher airspeeds in very strong updraft i.e. needs to increase power losses by flying faster to hold enforce zero flight path angle in cruise. However, as can be seen in Fig. 7 this effect is reduced in climbing flight, as excess power is converted to altitude rate. For most efficient flight, this should be done also in cruise, allowing the aircraft to leave the prescribed flight path. Increasing the resolution had no effect on variant B, showing that the numerical approach is adequate for this variant. For variants A and C the increased resolution lead to smoother speed-to-fly references.

4.2. Discussion of Variants

Investigating three different degrees of freedom in the flight path and speed optimization, the resultant speeds

with variant A are close to the aerodynamic optimum of best glide respectively minimal drag (MD) that is flown with lift coefficient and flight speed of

$$(34) C_{L,MD} = \sqrt{\frac{C_{D0}}{k}}$$

(34)
$$C_{L,MD} = \sqrt{\frac{C_{D0}}{k}}$$

$$V_{MD} = \sqrt{\frac{2mg}{\rho S \sqrt{\frac{C_{D0}}{k}}}}$$

which evaluates to 34.3 m/s at sea level, with the parameters given in Tab. 1, Without minimum throttle specification, analysed from strong updraft to downdraft variant A results in decreasing flight path angles that can be negative. However, this only holds until around zero vertical wind at which point power, flight path angle the optimal speed increase rapidly, almost in a bang-bang type control. The speed increase is similarly to combination (B) in downdraft. With combination (B), holding a prescribed flight path angle with optimal airspeeds shows that in strong updraft higher airspeeds than the minimum drag airspeed are selected, similar to glider pilots increasing speed when following subsequent strong updrafts. However, range could be improved if the flight path requirement is relaxed in strong updraft such that low airspeeds in strong updraft increase the altitude gain. With medium updraft strength, variant B evaluates to airspeeds close to the best climb rate speed V_y . With the given aircraft parameters, the best rate of climb speed Vy [36] is at 26.1 m/s at sea level.

$$(36) C_{L,Vy} = \sqrt{\frac{3C_{D0}}{k}}$$

(36)
$$C_{L,Vy} = \sqrt{\frac{3C_{D0}}{k}}$$

$$V_{Vy} = \sqrt{\frac{2mg}{\rho S \sqrt{\frac{3C_{D0}}{k}}}}$$

Variation C evaluates to a somewhat higher airspeed - using the 75 % power reference. Differences in airspeeds to analytical predictions based solely on aerodynamic properties can be rooted to both using a efficiency model, mainly the propeller model, and to the optimization also taking into account the horizontal distance travelled in climb, arriving at a compromise of climb rate and airspeed.

Based on negligible performance differences in statistical analysis, variation B was chosen for further investigations in vertical gust and in flight plan following. The precision of the performance model in matching a nonlinear simulation model that uses manufacturer data tables has been demonstrated as both gust response closely held the altitude reference and mission simulations have shown good waypoint tracking. Gust reaction of the control approach with fixed flight path angle has shown to establish the reference of horizontal flight. Initial altitude loss in downdraft and altitude gain in updraft are visible - a result of the throttle being evaluated for quasi-steady conditions as accelerations and vector changes are not considered in the model of speed-to-fly analysis. The increased airspeed reference in a downdraft gust allowed to cover more range with the same consumption, only

at negligible altitude loss. For random turbulence with zero mean vertical wind, this control should establish the reference flight path in the long term. But, deviations from the planned flight path can arise. For variant C, to reach the flight plan in medium zero vertical turbulence, a reference for the power (static power reference) should be given. Full freedom to optimize will lead to more interception behaviour. The method A can be modified to include the flight plan angle used in B as minimum requirement. The interception logic is described in [26]. It is possible to fly this way, but may not be intuitive.

The aircraft speed controller has a time constant of 6.67 s, such the updating the speed-to-fly at simulation rate is not necessary. Speed following behaviour generally is time delayed as the aircraft controller was designed to comply with robustness metrics and pilot The used update rate that is slower than the airspeed controller time constant would allow an integration without aircraft controller - with the pilot to follow the reference settings manually.

Range gains in turbulence are not guaranteed as the aircraft reacts slow because of inertia and flight controller gains that are selected to comply with certification and passenger comfort needs. Statistical analysis has shown that following local minima of optimal airspeed and power does not necessarily result in the global optimum of flight speeds in varying conditions. Additionally, in real flight and aside from statistical evaluation, wind is a function of position and altitude. Because of this fact, the problem of optimal aircraft power setting, thus flight speed and altitude rate does not have optimal substructure. This issue can be approached by combining the optimization with a flight plan generation function that takes wind into account.

An SoC-dependent modelling of battery energy consumption was established to find the best climb and cruise setting. The impact of battery characteristics as Peukert effect, voltage drop under load and battery resistance on the optimal flight condition was minor, only visible with using variant A which has freedom to optimize airspeed, throttle and the flight path. However, in this variant A the optima for best range flight in zero wind largely changes when excluding battery effect, with almost both the throttle setting and flight path angle doubled. This results in much higher climb rate as when including the battery model. Similar findings that battery modelling reduces climb in optimal flight have been stated by Settele [24], whose performance criterion was expanded in this work to include wind in both the thrust computation and therefore the evaluation of the propulsion efficiency as well as the ground speed. This method has both the general effect to adapt and compensate non-perfect horizontal wind forecast data and to benefit from vertical wind by reducing flight speed in updraft and flying faster in downdraft, thus both increasing the percentage of flight in updraft.

5. CONCLUSION

This work extends the research into battery powered best range flight with a graphical description including 3D-

11 ©2024

wind. The method is shown to integrate with flight plan path angle references. Such the methodology is usable for any powered condition including cruise and climb. Additionally, the method sweeps the operation points given in manufacturer data (propeller, engine), making it generally applicable.

Three different degrees of freedom were investigated, namely variant A free to optimize flight path angle, throttle and airspeed dependent on horizontal wind and wind direction as well as vertical wind, variant B fixing the flight path angle and variant C fixing throttle. Gained altitude was evaluated to possible glide range. In zero wind variant A indicates an optimum at a climb angle with corresponding throttle. This leads to the conclusion that with the given aircraft parameters a sawtooth flight tactic switching between climb and glide is most beneficial. For comparison, this optimum has been used to initialise the other variants B and C. A statistical evaluation with Gaussian wind distribution has shown that there is no disadvantage in using variant B or C over A. Following, variant B has been chosen to demonstrate a gust response that increased range while not increasing consumption compared to level flight with fixed airspeed. A coulumb-counting method in combination with a battery model for voltage, resistance and the effect of the discharge current has been integrated. Battery effect has shown to change the zero-wind optimum of variant A (full degrees of freedom in optimization) by reducing optimal throttle setting and climb angle. However the effect of the discharge current on usable battery capacity (Peukert-effect) has only been validated with constant discharge, and as such is only applicable to fixed power cruise. Changing state of charge values did not influence the results. However, if the battery configuration changes, to increased internal resistance or lower voltages, the optimization is readily able to account for resultant influences.

The resultant optimal cruise and climb settings for best range differ from the known solution of minimal drag airspeed when wind is encountered and from the solution of a somewhat faster Carson travel speed described in literature. Good coupling of variant B to an optimized sawtooth flight plan has been demonstrated in mean wind as well as with turbulence.

As static range evaluation in horizontal wind has shown, for slow electric aircraft the travel speed should take into account the wind conditions and a propulsion efficiency characteristic which favours flying close to the aerodynamic optimum should be chosen, making cruise and climb flight even slower. It is expected this holds until the energy density of batteries is increased significantly.

ACKNOWLEDGMENTS

The work presented in this paper was funded by the German Federal Ministry for Economic Affairs and Climate Action (BMWK) due to a resolution of the German Federal Parliament within the scope of the LuFo VI-1 project STELAR (grant number 20Q1962C). The authors gratefully acknowledge this support.

Contact address:

spark@tu-berlin.de

References

- Mukhopadhaya and Per-[1] J. В. Graver. formance of analysis regional elechttps://theicct.org/wptric aircraft. content/uploads/2022/07/global-aviationperformance-analysis-regional-electric-aircraftjul22-1.pdf-1.pdf, 2022.
- [2] S. Sahoo, X. Zhao, and K. Kyprianidis. A review of concepts, benefits, and challenges for future electrical propulsion-based aircraft. *Aerospace*, 7(4):44, 2020. DOI: 10.3390/aerospace7040044.
- [3] L. M. Cardone, G. Petrone, S. de Rosa, F. Franco, and C. S. Greco. Review of the recent developments about the hybrid propelled aircraft. *Aerotecnica Missili & Spazio*, 103(1):17–37, 2024. DOI: 10.1007/s42496-023-00173-6.
- [4] B. J. Brelje and J.R.R.A. Martins. Electric, hybrid, and turboelectric fixed-wing aircraft: A review of concepts, models, and design approaches. *Progress in Aerospace Sciences*, 104:1–19, 2019. DOI: 10.1016/j.paerosci.2018.06.004.
- [5] M. Hepperle. Electric flight potential and limitations, 2012, STO-MP-AVT-209, https://elib.dlr.de/78726/1/MP-AVT-209-09.pdf.
- [6] Y. C. Zhang, O. Briat, L. Boulon, J.-Y. Deletage, C. Martin, F. Coccetti, and J.-M. Vinassa. Non-isothermal ragone plots of li-ion cells from datasheet and galvanostatic discharge tests. *Applied Energy*, 247:703–715, 2019. DOI: https://doi.org/10.1016/j.apenergy.2019.04.027.
- [7] I. Beyers, Α. Bensmann, and R. Hanke-Rauschenbach. Ragone plots revisited: methodology A review of and application across energy storage technologies. Journal of Energy Storage, 73:109097, 2023.DOI: https://doi.org/10.1016/j.est.2023.109097.
- [8] G. Avanzini, E. L. de Angelis, and F. Giulietti. Optimal performance and sizing of a battery-powered aircraft. Aerospace Science and Technology, 59:132–144, 2016. DOI: 10.1016/j.ast.2016.10.015.
- [9] G. N. Barufaldi and M. A. V. Morales. Optimal range and endurance for electric aircraft driven by fixed-pitch propellers. *Journal of Aircraft*, 60(1):272–279, 2023. DOI: 10.2514/1.C036890.
- [10] M. Wang and M. Mesbahi. Energy management for electric aircraft via optimal control: Cruise phase. In AIAA Propulsion and Energy 2020 Forum, Reston, Virginia, 2020. American Institute of Aeronautics and Astronautics. DOI: 10.2514/6.2020-3565.

- [11] M. Kaptsov and L. Rodrigues. Electric aircraft flight management systems: Economy mode and maximum endurance. In *Journal of Guidance, Control,* and *Dynamics*, volume 41(1), pages 288–293. 2017. DOI: 10.2514/1.G002806.
- [12] M. Lindner, J. Rosenow, and H. Fricke. Aircraft trajectory optimization with dynamic input variables. CEAS Aeronautical Journal, 11(2):321–331, 2020. DOI: 10.1007/s13272-019-00430-0.
- [13] M. Lindner, J. Rosenow, T. Zeh, and H. Fricke. In-flight aircraft trajectory optimization within corridors defined by ensemble weather forecasts. *Aerospace*, 7(10):144, 2020.
- [14] P. Oettershagen, J. Förster, L. Wirth, G. Hitz, R. Siegwart, and J. Ambühl. Meteorology-aware multi-goal path planning for large-scale inspection missions with solar-powered aircraft. *Journal of Aerospace Information Systems*, 16(10):390–408, 2019. DOI: 10.2514/1.1010635.
- [15] J. W. Langelaan, A. Chakrabarty, A. Deng, K. Miles, V. Plevnik, J. Tomazic, T. Tomazic, and G. Veble. Green flight challenge: Aircraft design and flight planning for extreme fuel efficiency. *Journal of Aircraft*, 50(3):832–846, 2013. DOI: 10.2514/1.C032022.
- [16] B. H. Carson. Fuel efficiency of small aircraft. AIAA Aircraft Systems Meeting, California, 1980. DOI: 10.2514/3.57417.
- [17] D. F. Rogers, B. Martos, and F. Rodrigues. Low-cost accurate angle of attack system, DOT/FAA/TC-18/7. United States. Department of Transportation. Federal Aviation Administration. William J. Hughes Technical Center.
- [18] A. Nuic, D. Poles, and V. Mouillet. Bada: An advanced aircraft performance model for present and future atm systems. *International Journal of Adaptive Control and Signal Processing*, 24(10):850–866, 2010. DOI: 10.1002/acs.1176.
- [19] L. Jensen and R. J. Hansman. Fuel efficiency benefits and implementation consideration for cruise altitude and speed optimization in the national airspace system. volume ICAT-2014-04. MIT International Center for Air Transportation (ICAT) Department of Aeronautics Astronautics Massachusetts Institute of Technology Cambridge, MA 02139 USA, 2014.
- [20] A. Seitz, O. Schmitz, A. T. Isikveren, and M. Hornung. Electrically powered propulsion: comparison and contrast to gas turbines. In *Deutsche Luft- und Raumfahrtkonferenz 2012*. Deutsche Gesellschaft für Luft-und Raumfahrt-Lilienthal-Oberth eV, 2012.
- [21] F. Settele, F. Holzapfel, and A. Knoll. The impact of peukert-effect on optimal control of a battery-electrically driven airplane. *Aerospace*, 7(2):13, 2020. DOI: 10.3390/aerospace7020013.

- [22] G. Avanzini and F. Giulietti. Maximum range for battery-powered aircraft. *Journal of Aircraft*, 50(1):304–307, 2013. DOI: 10.2514/1.C031748.
- [23] M. Kaptsov and L. Rodrigues. Flight management systems for all-electric aircraft. In First Annual IEEE Conference on Control Technology and Applications, pages 2126–2131, [Piscataway, NJ], 2017. IEEE. DOI: 10.1109/CCTA.2017.8062767.
- [24] F. Settele. Strategien zur energieoptimalen Flugführung eines batterie-elektrisch angetriebenen Leichtflugzeuges. 2021, Phd. Thesis, Technical University of Munich.
- [25] J. W. Langelaan. Gust energy extraction for mini and micro uninhabited aerial vehicles. *Journal of Guidance, Control, and Dynamics*, 32(2):464–473, 2009. DOI: 10.2514/1.37735.
- [26] H. Spark, Y. Gazmawe, and F. J. Silvestre. Coupling of a trajectory optimisation strategy to local optimal setpoints for electric aircraft. In *Deutsche Luft- und Raumfahrtkonferenz 2012*. Deutsche Gesellschaft für Luft- und Raumfahrt - Lilienthal-Oberth e.V, 2023. DOI: 10.25967/610281.
- [27] R. Brockhaus, W. Alles, and R. Luckner. Flugregelung. Springer, 3. edition, 2011. ISBN: 978-3-642-01442-0.
- [28] T. Donateo, A. Ficarella, L. Spedicato, A. Arista, and M. Ferraro. A new approach to calculating endurance in electric flight and comparing fuel cells and batteries. *Applied Energy*, 187:807–819, 2017. DOI: 10.1016/j. apenergy.2016.11.100.
- [29] T. Donateo, C. L. de Pascalis, L. Strafella, and A. Ficarella. Off-line and on-line optimization of the energy management strategy in a hybrid electric helicopter for urban air-mobility. *Aerospace Science and Technology*, 113:106677, 2021. DOI: 10.1016/j.ast.2021.106677.
- [30] P. G. Anselma. Dynamic programming based rapid energy management of hybrid electric vehicles with constraints on smooth driving, battery state-of-charge and battery state-of-health. *Ener*gies, 15(5):1665, 2022. DOI:10.3390/en15051665.
- [31] N. Omar, P. Bossche, T. Coosemans, and J. Mierlo. Peukert revisited—critical appraisal and need for modification for lithium-ion batteries. *Energies*, 6(11):5625–5641, 2013. DOI: 10.3390/en6115625.
- [32] D. Doerffel and S. A. Sharkh. A critical review of using the peukert equation for determining the remaining capacity of lead-acid and lithium-ion batteries. *Journal of Power Sources*, 155(2):395–400, 2006. DOI: 10.1016/j.jpowsour.2005.04.030.
- [33] B. W. McCormick. *Aerodynamics, aeronautics, and flight mechanics*. J. Wiley and Sons, New York, N.Y., 1979. ISBN: 0471030325.

- [34] T. Jameson. A fuel consumption algorithm for unmanned aircraft systems. Technical report, U.S. Army Research Laboratory, ARL-TR-4803, White Sands Missile Range, NM 88002-5501.
- [35] H. Spark, P. J. González Ramirez, C. Ruwisch, W. Meyer-Brügel, and F. J. Silvestre. Development and experimental testing of flight path control using total energy control and siso control loops. In AIAA SCITECH 2023 Forum. American Institute of Aeronautics and Astronautics, Reston, Virginia, 01232023. DOI: 10.2514/6.2023-0104.
- [36] G. N. Barufaldi, M. A. V. Morales, and da Silva, R. G. A. Optimal climb performance of electric aircraft for minimal charge consumption. In *AIAA Scitech 2020 Forum*. DOI: https://doi.org/10.2514/6.2020-0025.